The GALEX Ultraviolet Virgo Cluster Survey (GUViCS)

A. Boselli, Samuel Boissier, E. Voyer, L. Ferrarese, G. Consolandi, L. Cortese, P. Côté, J. C. Cuillandre, G. Gavazzi, S. Gwyn, et al.

HAL Id: cea-01429911

https://cea.hal.science/cea-01429911

Submitted on 9 Jan 2017

Astronomy & Astrophysics

The GALEX Ultraviolet Virgo Cluster Survey (GUViCS)

VI. The UV luminosity function of the Virgo cluster and its surrounding regions

A. Boselli[1], S. Boissier[1], E. Voyer[1], L. Ferrarese[2], G. Consolandi[3], L. Cortese[4], P. Côté[2], J. C. Cuillandre[5], G. Gavazzi[3], S. Gwyn[2], S. Heinis[6], O. Ilbert[1], L. MacArthur[7], and Y. Roehlly[1]

[1] Aix Marseille Université, CNRS, LAM (Laboratoire d'Astrophysique de Marseille), UMR 7326, 13388 Marseille, France
e-mail: [alessandro.boselli;samuel.boissier]@lam.fr
[2] NRC Herzberg Astronomy and Astrophysics, 5071 West Saanich Road, Victoria, BC, V9E 2E7, Canada
e-mail: laura.ferrarese@nrc-cnrc.gr.ca
[3] Universitá di Milano-Bicocca, piazza della scienza 3, 20100 Milano, Italy
[4] Centre for Astrophysics Supercomputing, Swinburne University of Technology, Mail H29-PO Box 218, Hawthorn VIC 3122, Australia
[5] CEA/IRFU/SAP, Laboratoire AIM Paris-Saclay, CNRS/INSU, Université Paris Diderot, Observatoire de Paris, PSL Research University, 91191 Gif-sur-Yvette Cedex, France
[6] Department of Astronomy, University of Maryland, Stadium Drive, College Park, MD 20742-2421, USA
[7] Department of Astrophysical Sciences, Princeton University, Princeton, NJ 08544, USA

ABSTRACT

We use the GALEX data of the GUViCS survey to construct the near-ultraviolet (NUV) luminosity function of the Virgo cluster over ~300 deg^2, an area covering the cluster and its surrounding regions up to ~1.8 virial radii. The NUV luminosity function is also determined for galaxies of different morphological types and $NUV - i$ colours, and for the different substructures within the cluster. These luminosity functions are robust vs. statistical corrections since based on a sample of 833 galaxies mainly identified as cluster members with spectroscopic redshift (808) or high-quality optical scaling relations (10). We fit these luminosity functions with a Schechter function, and compare the fitted parameters with those determined for other nearby clusters and for the field. The faint end slope of the Virgo NUV luminosity function ($\alpha = -1.19$), here sampled down to ~$NUV = -11.5$ mag, is significantly flatter than the value measured in other nearby clusters and similar to the field value. Similarly, $M^* = -17.56$ is one to two magnitudes fainter than measured in Coma, A1367, the Shapley supercluster, and the field. These differences seem to be due to the quite uncertain statistical corrections and the small range in absolute magnitude sampled in these clusters. We do not observe strong systematic differences in the overall NUV luminosity function of the core of the cluster with respect to that of its periphery. We note, however, that the relative contribution of red and blue galaxies at the faint end is inverted, with red quiescent objects dominating the core of the cluster and star forming galaxies dominating beyond one virial radius. This observational evidence is discussed in the framework of galaxy evolution in dense environments.

Key words. galaxies: clusters: general – galaxies: evolution – galaxies: interactions – galaxies: ISM – galaxies: star formation – galaxies: clusters: individual: Virgo

1. Introduction

The environment plays a fundamental role in shaping galaxy evolution. Since the seminal work of A. Dressler in the 1980s it became evident that galaxies in rich environments are systematically different from those located in the field. They are generally quiescent ellipticals and lenticulars, in contrast to the dominant population of star forming disc galaxies along the cosmic web (Dressler 1980; Binggeli et al. 1988; Whitmore et al. 1993; Dressler et al. 1997). At the same time it became clear that the physical properties of the star forming systems inhabiting rich environments such as clusters and groups are also systematically different from those of their isolated analogues with a reduced gas content and activity of star formation (e.g. Boselli & Gavazzi 2006).

Several physical processes have been proposed to explain the origin of these differences. They can be divided into two main families, those related to the gravitational interactions between galaxies or with the potential well of the cluster (tidal interactions – Merritt 1983; Byrd & Valtonen 1990, harassment – Moore et al. 1998) and those exerted by the hot and dense intracluster medium on galaxies moving at high velocity within the overdense region (ram pressure stripping – Gunn & Gott 1972, viscous stripping – Nulsen 1982, thermal evaporation – Cowie & Songaila 1977, starvation – Larson et al. 1980). These processes might start to become active well before galaxies enter rich clusters because these large dynamically bounded structures form through the accretion of smaller groups of galaxies (pre-processing; Dressler 2004).

The identification of the dominant environmental process affecting galaxy evolution can be done through the statistical comparison of the physical properties of galaxies in a wide range of densities from the core of rich clusters and compact and loose groups down to the field, cutting the studied samples into slices

of redshift to trace the time-evolution of the effects. These processes act on different timescales and are characterised by efficiencies that depend on the density of galaxies and of the intergalactic medium, the velocity dispersion within the structure, and the mass of galaxies. The identification of the perturbing process can also be done through the comparison of the radial and kinematic properties of the perturbed galaxies with the predictions of tuned models and simulations.

Thanks to its proximity (∼17 Mpc, Gavazzi et al. 1999; Mei et al. 2007) and to its unrelaxed structure indicating that it is still undergoing formation, the Virgo cluster has become the ideal target in the local universe for the study of the effects of the environment on galaxy evolution. The advent of large panoramic detectors made it possible to perform the observations of the whole Virgo cluster region in the optical bands by the NGVS survey (Ferrarese et al. 2012), in the 21 cm HI line by ALFALFA (Giovanelli et al. 2005), and in the infrared by *Herschel* (The HeViCS survey, Davies et al. 2010). We have recently completed a UV survey of the cluster over ∼300 deg² using the GALEX space observatory (the GUViCS survey; Boselli et al. 2011). Ultraviolet data are of particular interest to trace the content and distribution of the young stellar populations in late-type galaxies (e.g. Kennicutt 1998; Boselli et al. 2009), and the one of the very evolved stars in quiescent systems (O'Connell 1999; Boselli et al. 2005a). For these reasons the UV data are critical to trace short-term variations in the star formation activity of late-type systems such as those encountered in galaxies freshly infalling in rich clusters (e.g. Boselli et al. 2006, 2008a,b, 2014a,b; Hughes & Cortese 2009; Cortese & Hughes 2009). The UV data extracted from this survey have been recently published in Voyer et al. (2014), and the study of the physical properties of Virgo cluster galaxies derived from a multifrequency analysis have been presented in Boselli et al. (2014a). In two other companion papers we presented the study of the extraplanar star formation activity of a few gas stripped galaxies in the cluster (Boissier et al. 2012) and of the diffuse Galactic emission of the UV scattered light in the Virgo direction (Boissier et al. 2015). In the present work we derive and study the UV luminosity function of the Virgo cluster and its surrounding regions. This work is thus an extension of the study presented in Boselli et al. (2011), where the UV luminosity function was derived only for the central 12 deg². The luminosity function is a statistical tool widely used to study the mean properties of large samples of galaxies. Often used in other wavelength domains, it has been derived at rest frame in the GALEX UV bands only for the general field (Wyder et al. 2005) and for a few other nearby clusters (Coma, Cortese et al. 2008; Hammer et al. 2012; A1367, Cortese et al. 2005; Shapley, Haines et al. 2011). Compared to these previous works, the UV luminosity function derived from the GUViCS survey has the great advantage of including a significantly large number of objects with direct redshift measurements, of sampling a much wider range in galaxy density, from the core of the cluster out to the periphery (∼2 R_{vir}), and of including the dwarf galaxy population ($NUV \lesssim -11.5$ mag). Dwarf systems are of particular interest in the study of the effects of the environment on galaxy evolution since they are fragile objects easily perturbed because of their shallow potential well (e.g. Boselli & Gavazzi 2014).

The paper is structured as follows. In Sect. 2 we describe the dataset used in this analysis, while in Sect. 3 we explain the different techniques used to identify Virgo cluster members. The UV luminosity function is derived in Sect. 4 and analysed in the framework of galaxy evolution in rich environments in Sect. 5.

2. The data

The GUViCS survey has covered the Virgo cluster in the region between 12 h ≤ RA ≤ 13 h and 0° ≤ dec ≤ 20°. In this region the sky coverage is 94% (Boselli et al. 2014a) at the depth of the All Imaging Survey (AIS), where the completeness is 20 mag, and 65% at the depth of the Medium Imaging Survey (MIS; 21.5 mag)[1]. Unfortunately, because of a failure of the far-ultraviolet (FUV) detector, this survey was completed only in the NUV. The analysis presented in this work will thus be limited to this band. The number of NUV detected sources in the covered region is more than 1.2 million (Voyer et al. 2014) and includes Milky Way stars, nearby galaxies, and background sources. To construct the NUV luminosity function of the Virgo cluster and of its surrounding regions we have to count the number of galaxies in a given volume down to a limiting magnitude. For consistency with our previous works we consider as Virgo members those galaxies with a recessional velocity $vel \leq 3500$ km s⁻¹. This limit was chosen to include all the objects belonging to the different cluster substructures and their surrounding regions (e.g. Boselli et al. 2014a). As limiting magnitude we adopt $NUV = 20$ mag. Down to this magnitude the catalogue is 100% complete over the ∼300 deg² covered by the survey.

Voyer et al. (2014) provide integrated magnitudes for extended sources (UV-VES catalogue) included in the widely known catalogues of nearby galaxies (e.g. NGC, UGC, IC, VCC) for a total of 1770 galaxies. These magnitudes were extracted with the FUNTOOLS analysis package on DS9 using manually defined apertures adjusted to fit the full UV profile of each target galaxy. The same procedure was adopted for all the sources identified as Virgo cluster members using spectroscopic redshifts. This procedure is necessary for extended sources where the automatic GALEX pipeline often does not recognise the extended nature of the galaxies from the point-like structure of HII regions, galaxy nuclei, or complex high surface brightness features present in star forming systems. For the other sources, NUV fluxes have been taken from the catalogue of point-like objects (UV-VPS) of Voyer et al. (2014). Down to the limiting magnitude of $NUV = 20$ mag this catalogue includes 33026 objects. These are generally faint objects where the NUV magnitudes extracted from the pipeline are accurate enough for the purpose of this work. As clearly shown in Boselli et al. (2011) (Fig. 7), the difference between extended magnitudes and those extracted from the standard GALEX pipeline optimised for point-like sources is ≲0.3 mag whenever $NUV \gtrsim 17$ mag. Ultraviolet magnitudes are corrected for Galactic attenuation using the Schlegel et al. (1998) map combined with the Fitzpatrick & Massa (2007) extinction curve. Given the high Galactic latitude of the Virgo cluster, these corrections are low ($A(NUV) \lesssim 0.4$ mag; Boissier et al. 2015).

For all galaxies at the distance of Virgo ($vel \leq 3500$ km s⁻¹) we also extracted 22 μm WISE fluxes necessary for the dust internal attenuation corrections. These fluxes were extracted from the original WISE fits images with the same procedures used for the UV data, consistently with Boselli et al. (2014a). The dust extinction correction is performed following the prescription of Hao et al. (2011). Near-ultraviolet (NUV) corrected data are used to estimate the star formation rate (SFR) in star forming galaxies, again using the prescription of Hao et al. (2011).

---

[1] The coverage is less than 100% because of the presence of a few bright young stars, which were expressly avoided during the survey because they saturate the UV detector.

Distances are necessary to calculate absolute magnitudes. For consistency with our previous works, distances are determined assuming the mean distance of the different cluster subgroups (see Table 3 in Boselli et al. 2014a). Galaxies at the periphery of the cluster are all assumed at 17 Mpc, the distance of the main body of Virgo.

3. Identification of Virgo members

The construction of the NUV luminosity function needs first the identification of all galaxies at the distance of Virgo, among the UV detections with $NUV \leq 20$ mag. This is done using spectroscopic redshift whenever available (see Sect. 3.1), otherwise photometric relations (Sect. 3.2) or statistical considerations (Sect. 3.3).

3.1. Identification based on spectroscopic data

Voyer et al. (2014) has cross-matched all the UV detections with the spectroscopic catalogues available online (NED[2], SDSS DR9[3]). For these objects the spectroscopic information can be easily used to identify Virgo members ($vel \leq 3500$ km s^{-1}). Out of the 1770 galaxies listed in the extended source catalogue, 688 galaxies match these criteria. There are, however, 34 extended galaxies with $NUV \leq 20$ mag but without any redshift information. Among these, we identify the possible cluster members using the same procedures adopted for the other galaxies included in the UV point source catalogue (see below).

As previously mentioned, down to $NUV \leq 20$ mag the majority of the point-like detected objects are not Virgo cluster members, but rather Galactic stars and background sources. Given the poor angular resolution of the GALEX images (~4–5 arcsec), the separation of point-like stars from extended galaxies requires the use of optical images of better quality. Considering the typical UV-optical colour magnitude relation of galaxies in the Virgo cluster (e.g. Boselli et al. 2014a), a cut at $NUV = 20$ mag roughly corresponds to a cut in the SDSS g band of ~19 mag for the blue star forming objects and $g \sim 16$ mag for the quiescent dwarf ellipticals. At this depth the SDSS is complete in terms of total magnitude and surface brightness and can thus be used for this purpose. Out of the 33 026 GUViCS point-like sources with $NUV \leq 20$ mag, 32 277 (98%) have an optical counterpart in the SDSS; the 749 objects without a SDSS counterpart are mainly ghosts of saturated stars, HII regions in resolved galaxies, or multiple systems unresolved in the UV images. About one-third of the sources with a counterpart (7532) are photometrically identified as galaxies in the SDSS (SDSS_phot_ObjType = 3). We have cross-matched these objects with the SDSS DR12 spectroscopic catalogue, with NED, and with eBOSS through the DR12 SDSS finding chart tool. Spectra are available for 5620 galaxies (75% of the sample). Their optical image on the SDSS DR12 finding chart revealed, however, that a significant fraction of them are bright stars. Generally saturated, they are extended on the SDSS image and thus misclassified as galaxies by the automatic SDSS pipeline. Among the bona fide galaxies of the UV-VPS catalogue of Voyer et al. (2014) with available redshift, we identify 125 objects with $vel \leq 3500$ km s^{-1}. Five of these, however, are left out of the sample because the NUV magnitudes determined using our ad hoc procedures for extended sources are below the limiting

value of $NUV = 20$ mag. The resulting sample of Virgo cluster members determined using spectroscopic data thus consists of 808 galaxies.

3.2. Identification using optical NGVS scaling relations

The identification of Virgo members among those objects without any spectroscopic data is critical in the determination of the luminosity function. The membership criteria adopted by the NGVS, fully described in Ferrarese et al. (2015), give the probability that a galaxy belongs to Virgo according to its location in a multiparameter space defined by a combination of galaxy structural parameters, photometric redshifts (Raichoor et al. 2014), and an index measuring the strength of residual structures in images created by subtracting a best fitting Sersic model from each galaxy. The exact combination of axes in this space was selected to allow for maximum separation of known (mostly spectroscopically confirmed) Virgo members and background sources, the latter identified in control fields located at three virial radii from the cluster centre. The NGVS covers 104 square degrees, and its entire footprint is mapped by GUViCS. We thus cross-matched the GUViCS UV-VPS catalogue with the NGVS catalogue of Virgo members identified using their photometric parameters and found 10 UV sources identified as Virgo members in the NGVS. We assume all these objects at a distance of 17 Mpc, the typical distance of Virgo and of its surrounding regions. The depth of the NGVS survey, which is 3 mag deeper than the SDSS in terms of surface brightness sensitivity, guarantees that all UV detected galaxies down to $NUV \leq 20$ mag have an optical counterpart.

3.3. Identification using statistical estimates oustide the NGVS footprint

The NGVS covers Virgo out to one virial radius, for a total of 104 square degrees. To identify Virgo members in the GUViCS areas beyond the NGVS boundaries, and in the absence of spectroscopic information, we must therefore resort to statistical arguments. In the GUViCS UV-VPS catalogue there are 1884 UV galaxies without any membership information. We drop those located within the NGVS footprint, reducing the sample of objects with no available membership information to 1155 sources. We then use three different statistical methods to estimate the number of potential members among these galaxies.

3.3.1. Statistical correction based on NGVS results

If 10 galaxies with no redshift in the NGVS footprint (104 deg^2) are identified as Virgo members using criteria adopted by the NGVS and the density of galaxies is conserved over the surveyed region, 20 extra objects are expected to be present in the remaining ~200 deg^2 covered by GUViCS. Since the NGVS observed the central region of the cluster where the density is at its maximum, this number should be considered as an upper limit.

3.3.2. Statistical correction based on redshift measurements

Out of the 5620 galaxies in the VPS catalogue of Voyer et al. (2014) with spectra in the 300 deg^2 of the GUViCS survey only 125 have $vel \leq 3500$ km s^{-1}. If we assume that the same ratio of members/background galaxies is conserved among those objects without any spectroscopic information (1884), we would

---

thus expect 42 new members. This number drops to 30 if we limit this comparison in the region located outside the NGVS footprint corresponding to the cluster periphery (90/3452).

3.3.3. Statistical correction based on GALEX-SDSS scaling relations

An alternative method for identifying possible members was first proposed by Boselli et al. (2011). For the same reasons given above, cluster galaxies populate different regions in the optical and UV surface brightness vs. observed magnitude relations and can thus be distinguished using their photometric parameters. Unfortunately, the relations proposed by Boselli et al. (2011) are not sufficiently accurate to identify Virgo members among quiescent dwarf galaxies such as those located in the central 12 deg^2 analysed in that work. Here we propose an alternative technique based on three different scaling relations ($\Sigma(r)$ vs. r mag, $g-i$ vs. $NUV-g$, and $NUV-i$ vs. i mag, where $\Sigma(r)$ is the mean surface brightness within the half-light radius[4,5]), which we demonstrate to be fairly efficient at rejecting a significant number of background objects also among star forming systems such as those detected in the outer regions of the cluster (see Fig. 1). Despite their relative low scatter, these relations are unfortunately not sufficiently accurate for an unambiguous identification of cluster members and thus need to be combined with statistical tests.

These scaling relations are determined using either the Extended Virgo Cluster Catalogue (EVCC, Kim et al. 2014) or the GUViCS catalogue of galaxies analysed in Boselli et al. (2014a). The EVCC catalogue was chosen because it includes galaxies at the same distance as Virgo ($vel \leq 3000$ km s^{-1}), it has both star forming and quiescent galaxies, and provides structural parameters comparable to those listed in the GUViCS point-like catalogue of Voyer et al. (2014). The EVCC catalogue is used to determine the $\Sigma(r)$ vs. r apparent magnitude relation. Unfortunately, the EVCC catalogue does not include UV magnitudes and thus cannot be used in the $g-i$ vs. $NUV-i$ colour–colour and the $NUV-i$ vs. i relations. For these UV-based relations, we use the sample composed of Virgo cluster galaxies analysed in Boselli et al. (2014a) as a comparison sample. Galaxies are separated according to their morphological types (early- and late-type) and atomic gas content. For consistency, the Virgo cluster sample is limited to $NUV \leq 20$ mag.

Figure 1 shows the following:

a) A number of sources identified by the standard SDSS pipeline or by our visual inspection of the SDSS finding charts as galaxies are saturated stars. They have r-band surface brightnesses ~5 mag brighter than those of typical galaxies of similar magnitude, but are comparable to those of stars. We identify as possible members in the $\Sigma(r)$ vs. r mag plot all galaxies satisfying the condition $\Sigma(r) > 0.5 \times r + 12.4$. We note that this criterion is different and less strict than the one used in Boselli et al. (2014a) and that the number of rejected objects is relatively small. This difference is due to the fact that in the inner 12 deg^2. at faint magnitudes the population of Virgo members is strongly dominated by dwarf ellipticals with red colours. Thus, the difference in $\Sigma(r)$ with background star forming galaxies was more pronounced than

b) All Virgo cluster members avoid the region above the $g-i = 0.6 \times (NUV-g) - 0.2$ and $g-i = 0.23 \times (NUV-g) + 0.45$ relations in the $g-i$ vs. $NUV-g$ colour–colour diagram. These regions are populated mainly by background sources.
c) The sharp cut in the $NUV-i$ vs. i colour–magnitude relation is due to the adopted cut in NUV. This relation, however, shows that all identified members have observed i magnitudes ≤ 18.

These relations can be combined with a limit on the photometric redshift, accurately determined on these bright sources, to reject background galaxies. This is done by removing all objects with $z_{\text{photNN}} \geq 0.1$, where NN stands for the Neural Network (NN) photometric redshift definition (D'Abrusco et al. 2007). This cut in photometric redshift, which corresponds to that adopted by Boselli et al. (2011) for the rejection of background galaxies in the inner 12 deg^2 of the cluster, has been chosen to maximise the number of background rejected objects and minimise the exclusion of possible members. With this new selection criteria, the sample of possible members outside the NGVS footprint drops to 264 objects. The number of spectroscopically confirmed Virgo galaxies satisfying the same photometric criteria is 75/90 (83.3%), while that of members over background objects 75/1636 (4.6%). We thus expect that 15 out of the 264 galaxies satisfying the criteria are at the distance of Virgo.

3.3.4. Applied statistical correction

The three statistical methods described above give consistent results. We thus include 15 extra objects to those already selected spectroscopically (see Sect. 3.1) or using NGVS data (Sect. 3.2) in the determination of the NUV luminosity function. The distribution of the 264 galaxies selected according to Fig. 1 is used to make the appropriate statistical correction as a function of the NUV absolute magnitude in the determination of the NUV luminosity function (see Fig. 2). These 15 galaxies are all assumed to be at a distance of 17 Mpc. The correction is more important at faint luminosities. Figure 1 also shows that these statistically added galaxies, all located in the outer regions of the cluster, are blue.

The resulting sample is thus composed of 808 spectroscopically confirmed sources; 10 objects were identified at the distance of the Virgo cluster using NGVS based scaling relations and 15 extra objects were added for statistical considerations for a total of 833 galaxies. This indicates that the determination of the NUV luminosity function is very robust against statistical uncertainties, making the Virgo cluster the ideal target for such studies in the nearby universe (e.g. Rines & Geller 2008).

3.4. Possible biases

The identification of galaxies through automatic pipelines is first done using surface brightness criteria. Low surface brightness, extended systems are barely detectable even if their integrated magnitude is above the limiting magnitude requested for the completeness of the survey. These systems might thus be potentially missed in the GUViCS survey. This effect, however, should be limited because 65% of the Virgo cluster region has been mapped at the depth of the GALEX MIS (~1500 s) where the completeness limit of 22.7 mag (Morrissey et al. 2007) is significantly deeper than the one adopted in this work. At this
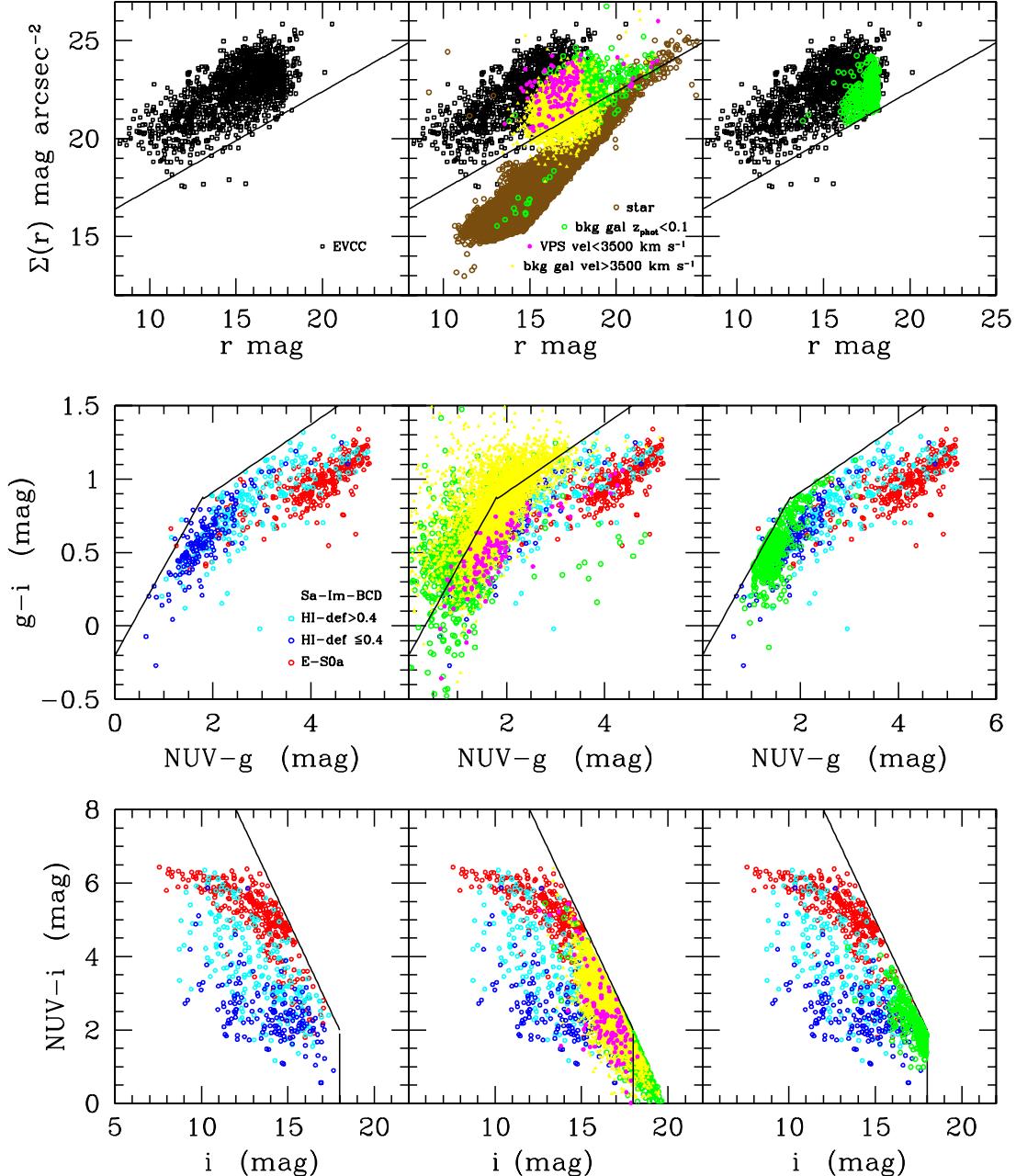
---

[4] The GUViCS catalogue lists the Petrosian half-light radius, while the EVCC the Kron half-light radius. We have checked that these radii are consistent for galaxies belonging to both samples.
[5] All values are corrected for Galactic extinction. These relations are also different from those adopted by Ferrarese et al. (2015) based only on optical data.

Fig. 1. Scaling relations used to identify Virgo cluster possible members: $\Sigma(r)$ vs. r (*upper row*), $g - i$ vs. $NUV - g$ (*middle row*), and $NUV - i$ vs. i (*lower row*). *Left panels*: scaling relations of spectroscopically confirmed Virgo members included in the extended source GUViCS catalogue. The black empty squares indicate the local EVCC galaxies. The red, cyan, and blue empty circles in the middle and lower panels indicate the early-type and late-type galaxies, these last selected according to their HI-gas content (HI-def ≤ 0.4, blue symbols; HI-def > 0.4, cyan symbols). The black solid lines indicates the limits in the different scaling relations used to identify possible Virgo cluster members. *Central panels*: relations drawn when all optically identified galaxies with $NUV < 20$ mag from the GUViCS VPS catalogue are included. Stars, plotted only in the central upper panel, are indicated with a brown open circle. VPS galaxies with *vel* ≤ 3500 km s^{-1} are indicated with magenta filled dots, spectroscopically confirmed background sources with filled yellow triangles, while potential members with photometric redshift ≤0.1 with green empty circles. *Right panels*: scaling relations of spectroscopically confirmed Virgo members (as in the left panels) with candidate members from the VPS catalogue selected using the criteria given in Sect. 3.3.3 (green empty circles). All these relations are determined using UV data corrected for Galactic dust attenuation.

depth, low surface brightness features can be detected down to ~28.5 mag arcsec^{-2} (e.g. Boselli et al. 2005b). Furthermore, Voyer et al. (2014) have systematically checked the UV images of all the optically selected VCC galaxies. The analysis presented in Boselli et al. (2011) revealed that most of the UV detected galaxies used to construct the UV luminosity function down to $NUV = 21$ mag in the central 12 deg^2 of Virgo (1 mag below the UV limit adopted in this work) have a counterpart in the VCC catalogue. This central region, however, is dominated by quiescent red galaxies, thus bright in the optical bands if detected in the NUV.

None of the three extremely low surface brightness extended galaxies ($\Sigma(g) \sim 28$ mag arcsec^{-2}) recently discovered by Mihos et al. (2015) in the core of the Virgo cluster has been detected by GALEX. Given their total magnitude ($g \gtrsim 17$ mag), and the typical colour of quiescent dwarf ellipticals ($NUV - g \gtrsim 3$ mag),
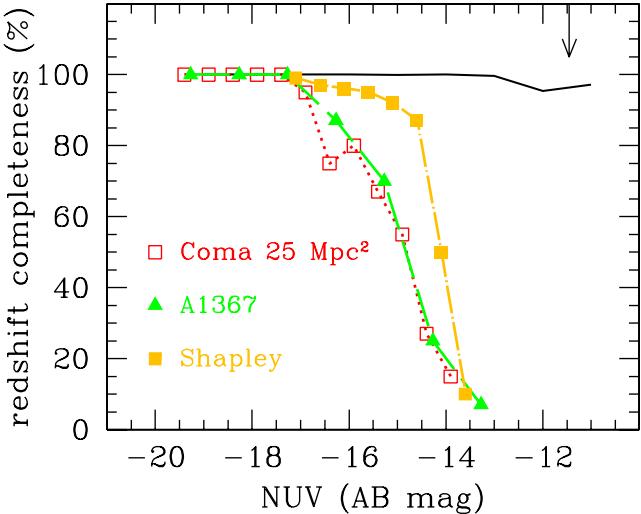
Fig. 2. NUV redshift completeness of the GUViCS sample compared to that of Coma (red open squares; Cortese et al. 2008), A1367 (green filled triangles; Cortese et al. 2005), and Shapley supercluster (orange filled squares; Haines et al. 2011). The vertical arrow shows the photometric completeness limit of the present survey ($NUV = -11.45$).

Fig. 3. NUV luminosity function of the Virgo cluster (filled dots). The best fit Schechter function (black solid line) is compared to that determined for the central 12 deg^2 of the cluster by Boselli et al. (2011) at a limiting absolute magnitude of $NUV \leq -10$ (cyan dot-dashed line) and $NUV \leq -13$ (cyan dotted line), and to that of the Coma cluster (red dotted line, from Cortese et al. 2008), A1367 (green long-dashed line, Cortese et al. 2005), Shapley supercluster (orange dot-dashed line; Haines et al. 2011) and the field (blue dashed line, Wyder et al. 2005). The different luminosity functions have been normalised to approximately the same number of objects above the completeness limit of each cluster for a fair comparison. The vertical arrow shows the completeness limit of the present survey ($NUV = -11.45$).

we would expect that their total NUV magnitude is $\gtrsim$20 mag, thus below the limiting magnitude adopted for the determination of the UV luminosity function. Less extreme objects such as those observed in Coma by van Dokkum et al. (2015) and Koda et al. (2015) are easily detected by the NGVS and are thus considered in the NUV vs. optical cross-identification. The NGVS footprint largely overlaps with the VCC region, and has been observed in four photometric bands (*ugiz*) at a point-source depth of $g \sim 25.9$ mag and a surface brightness limit $\Sigma(g) \sim 29$ mag arcsec^{-2} (Ferrarese et al. 2012). This limit in surface brightness is roughly 4 mag below the value reached by the VCC (Ferrarese et al. 2012). Among the UV detected galaxies with $NUV < 20$ mag, 43 objects identified as Virgo members from spectroscopic measurements or using the NGVS scaling relations have an optical counterpart in the NGVS but not in the VCC. Outside the NGVS footprint, optical data are available from the SDSS. Its sensitivity in surface brightness is ~26 mag arcsec^{-2}, thus ~one mag better than the VCC. At the depth of the present survey ($NUV < 20$ mag) most of the UV detected sources have a counterpart in the SDSS (98%, see previous section); it is thus likely that the number of Virgo cluster galaxies without an optical counterpart missed in the present analysis is low. A rough estimate of this number can be derived thanks to the NGVS. If the density of galaxies is conserved all over the GALEX surveyed region and if we assume that the sensitivity of the VCC is comparable to that of the SDSS, we expect to miss 86 galaxies (2×43). Once again, this number should be considered as an upper limit because i) the density of galaxies significantly drops outside the central regions of the cluster; and ii) the SDSS is ~1 mag more sensitive in surface brightness than the VCC. Furthermore, this number is comparable to the number of galaxies statistically added in the previous section (15). We thus expect that the number of faint galaxies missed for their low surface brightness in UV is small compared to the total number of galaxies.

Another possible source of uncertainty is the presence of extremely compact extragalactic sources erroneously identified as stars in the SDSS optical images whose typical resolution is of the order of ~1 arcsec. Typical examples are the ultra compact
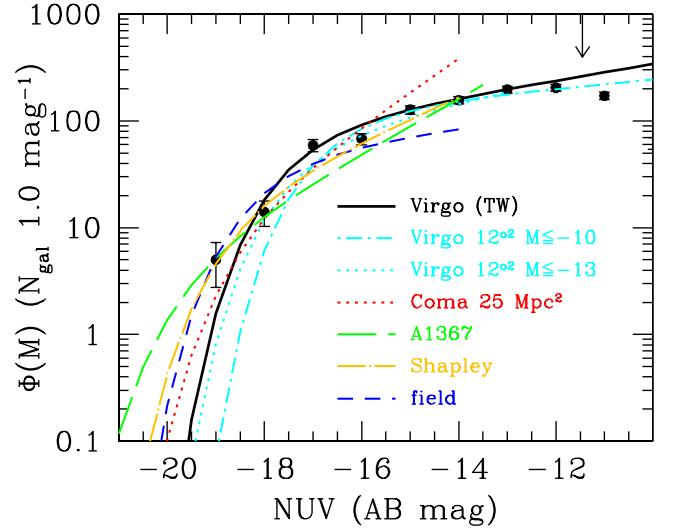
dwarf galaxies (UCDs), a population of extragalactic sources with characteristics in between those of compact elliptical galaxies and globular clusters (Hilker et al. 1999; Drinkwater et al. 2000; Zhang et al. 2015). These sources, however, have NUV apparent magnitudes below the $NUV = 20$ mag limit because of their relatively red colours (Boselli et al. 2011) and should not be counted in the determination of the NUV luminosity function of Virgo. Blue compact dwarf galaxies (BCD), characterised by an intense star formation activity, have angular dimensions of $\gtrsim$10 arcsec at the distance of Virgo and are thus fully resolved by the SDSS. They are thus included in the present analysis.

4. NUV luminosity function

4.1. NUV luminosity function of the whole cluster

Figure 3 shows the NUV luminosity function of the whole cluster determined over the 300 deg^2 of the GUViCS survey. The number of galaxies per bin of absolute NUV magnitude[6] are listed in Table 1. Given that the virial radius R_V of cluster A (the main substructure in Virgo) is 5.38 degrees (McLaughlin 1999; Ferrarese et al. 2012, corresponding to 1.60 Mpc at the distance of 17 Mpc), this luminosity function is representative of the cluster up to ~1.8 virial radii. For comparison with other clusters, we note that the core radius of Virgo is of 0.45° (130 kpc; Boselli & Gavazzi 2006). We fit the data with a Schechter function with parameters given in Table 2. Following Ilbert et al. (2005) we use the MINUIT package of the CERN library (James & Roos 1995) to minimise the likelihood (MIGRAD procedure), to obtain the non-parabolic error for each parameter (MINOS procedure) and the error contour $\alpha - M^*$ (MNCONT procedure). The

---

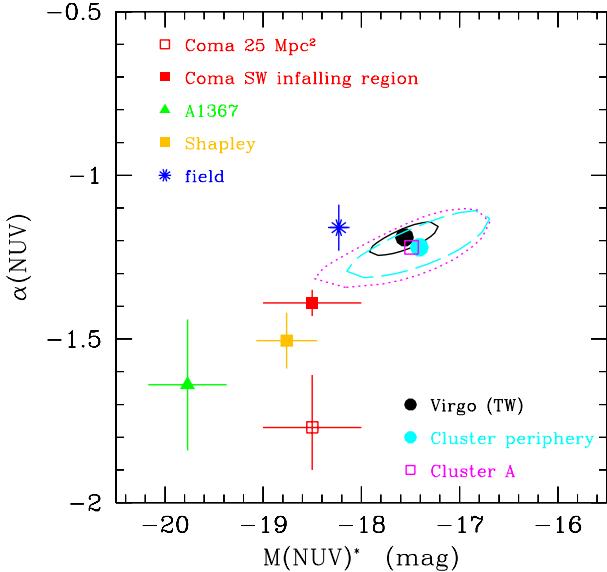[6] Corrected for Galactic attenuation.

Fig. 4. Comparison of the parameters obtained after fitting a Schechter function to the NUV luminosity function of the Virgo cluster (black filled circle), of Virgo cluster A (magenta open square), of the cluster periphery (cyan filled dot), to those determined in Coma over 25 deg$^{\circ 2}$ (red empty square, Cortese et al. 2008) or in its SW infalling region (red filled square, Hammer et al. 2012), in A1367 (green filled triangle, Cortese et al. 2005), in the Shapley supercluster (orange filled square, Haines et al. 2011), and the field (blue asterisk, Wyder et al. 2005). Contours indicate the 1σ probability distribution of the two correlated parameters.

Table 1. NUV luminosity function.

NUV	All	Blue	Green	Red
−20	–	–	–	–
−19	5	5	–	–
−18	14	14	–	–
−17	59	48	2	9
−16	68	45	13	10
−15	127	69	18	40
−14	156	72	36	48
−13	196	70	47	79
−12	204	49	53	102

Notes. Number of objects.

parameters of the fit are compared to those determined for the central 12 deg^2 of Virgo by Boselli et al. (2011), for other clusters and for the field in Fig. 4.

The NUV luminosity function of Virgo is well fitted by a Schechter function with $M^* = -17.56$ and $\alpha = -1.19$. These values are close to those determined in the central 12 deg^2 by Boselli et al. (2011), but are significantly different from those determined in Coma (Cortese et al. 2008; Hammer et al. 2012), A1367 (Cortese et al. 2005), in the Shapley supercluster (Haines et al. 2011), or in the field (Wyder et al. 2005). The slope of the faint end of the NUV luminosity function of Virgo ($\alpha = -1.19$) is significantly flatter than that of Coma, A1367, or the Shapley supercluster ($\alpha - 1.5 / - 1.6$) as first seen by Boselli et al. (2011); however, the slope is comparable to the value determined in the field ($\alpha = -1.16$; Wyder et al. 2005). The value of M^* is ~1 mag fainter than in Coma, in the Shapley supercluster, and in the field, and 2 mag fainter than in A1367.

4.2. Luminosity function in the different cluster substructures

The comparison of the properties of the luminosity function determined in different environments, from the cluster periphery to the densest regions in the core of the cluster, are useful for statistically constraining the role played by the environment in shaping galaxy evolution. The determination of the statistical properties of the different cluster substructures, accreted at different epochs, is important in order to understand the role of pre-processing in the transformation occurring in cluster galaxies.

4.2.1. Cluster A vs. periphery

Thanks to the large number of objects, we can determine the NUV luminosity function separately for the core of the cluster and for its periphery (Table 3). Consistently with Boselli et al. (2014a), we select galaxies within cluster A as those objects with $vel < 3500$ km s^{-1} and with an angular distance from M87 $< 2.692°$, corresponding to half its virial radius. The periphery is composed of all galaxies with $vel < 3500$ km s^{-1} and an angular distance from M87 $> 6.1°$ (>1.1 virial radii from the main body of the cluster). The NUV luminosity functions of cluster A and of the cluster periphery, whose values are given in Table 3, are fitted with a Schechter function and are compared in Fig. 5, while the fitted parameters are given in Table 2. The fitted parameters for cluster A and for the periphery are compared to those determined for the whole cluster and for other clusters in Fig. 4.

Figures 4 and 5 and Table 2 show that the NUV luminosity function, as in Coma (Cortese et al. 2008), does not significantly change from the core of cluster A to the cluster periphery outside $\gtrsim 1.1 R_{vir}$.

4.2.2. Other cluster substructures

The luminosity function of the main body of the cluster (cluster A) determined within half of the virial radius R_{vir}, and that of the cluster periphery ($\gtrsim 1.1 R_{vir}$) can also be compared to those determined for the other cluster substructures (Table 3). This can only be done for cluster B and the W cloud, which have a sufficient number of objects. To increase the statistics in the remaining substructures, we combine their data according to the general properties of their members as determined in Boselli et al. (2014a). We thus combine cluster C and the W' cloud, which are dominated by quiescent objects, while the M cloud with the low-velocity cloud (LVC) which, on the contrary, are mainly composed of star forming systems. The comparison of the different NUV luminosity functions is shown in the lower panel of Fig. 5 and in Fig. 6, while the fitted parameters are given in Table 2. Despite the poor statistics, the comparison of the different luminosity functions suggests that these substructures have a flatter slope at the faint end than cluster A or the field. These trends, however, should be confirmed on stronger statistical basis.

4.3. Luminosity function as a function of morphological type

The sample can also be cut into different subclasses according to the morphological types of the galaxies (Table 4). This can be done either by using the accurate morphological classification given in the VCC (Binggeli et al. 1985) or in the EVCC (Kim et al. 2014), or by using the colour of galaxies as in Boselli et al. (2014a). As in our previous work, we select galaxies belonging to the red sequence, the green valley, and the blue cloud

Table 2. Best fitting parameters for the NUV luminosity function.

Sample	α	M^*	ϕ_*
Full sample	$-1.19^{+0.03}_{-0.03}$	$-17.56^{+0.23}_{-0.24}$	$88.40^{+16.33}_{-14.71}$
Red sequence	$-1.37^{+0.12}_{-0.10}$	$-16.57^{+0.70}_{-0.98}$	$24.93^{+20.59}_{-13.35}$
Green valley	$-1.21^{+0.10}_{-0.10}$	$-16.11^{+0.40}_{-0.42}$	$27.74^{+11.88}_{-9.42}$
Blue cloud	$-0.94^{+0.05}_{-0.05}$	$-17.51^{+0.25}_{-0.25}$	$85.24^{+15.40}_{-14.11}$
Late-type	$-1.07^{+0.04}_{-0.04}$	$-17.54^{+0.24}_{-0.25}$	$85.58^{+15.93}_{-14.42}$
Cluster A	$-1.22^{+0.08}_{-0.08}$	$-17.49^{+0.50}_{-0.58}$	$14.14^{+6.37}_{-5.19}$
Cluster periphery	$-1.22^{+0.07}_{-0.07}$	$-17.41^{+0.47}_{-0.48}$	$25.51^{+10.45}_{-8.03}$
Cluster A red sequence	$-1.25^{+0.24}_{-0.28}$	$-15.70^{+0.73}_{-2.79}$	$12.92^{+13.27}_{-12.92}$
Cluster A green valley	$-0.92^{+0.39}_{-0.51}$	$-15.23^{+0.72}_{-0.91}$	$10.81^{+9.62}_{-9.56}$
Cluster A blue could	$-0.76^{+0.16}_{-0.15}$	$-17.29^{+0.50}_{-0.64}$	$14.62^{+6.20}_{-5.45}$
Cluster A late-type	$-0.99^{+0.11}_{-0.11}$	$-17.41^{+0.50}_{-0.62}$	$14.13^{+6.11}_{-5.26}$
Cluster periphery red sequence	$-1.45^{+0.21}_{-0.16}$	$-23.97^{+7.25}_{-14.82}$	$0.12^{+4.46}_{-0.12}$
Cluster periphery green valley	$-0.71^{+0.55}_{-0.51}$	$-13.64^{+0.58}_{-0.79}$	$28.82^{+15.14}_{-17.29}$
Cluster periphery blue cloud	$-1.10^{+0.09}_{-0.08}$	$-17.32^{+0.56}_{-0.55}$	$24.99^{+11.06}_{-8.22}$
Cluster periphery late-type	$-1.15^{+0.08}_{-0.07}$	$-17.27^{+0.50}_{-0.53}$	$27.13^{+11.51}_{-8.83}$
Cluster B	$-1.12^{+0.11}_{-0.11}$	$-18.41^{+0.94}_{-0.92}$	$6.54^{+4.05}_{-3.11}$
W cloud	$-1.09^{+0.72}_{-0.17}$	$-15.94^{+2.13}_{-0.77}$	$12.77^{+36.81}_{-6.37}$
Cluster C + W' cloud	$-1.05^{+0.24}_{-0.19}$	$-17.71^{+1.38}_{-2.36}$	$5.28^{+6.10}_{-4.91}$
M cloud + LVC	$-0.93^{+0.24}_{-0.19}$	$-16.22^{+0.97}_{-1.05}$	$11.61^{+8.95}_{-5.91}$
NGVS footprint[a]	$-1.18^{+0.04}_{-0.04}$	$-17.50^{+0.26}_{-0.27}$	$58.78^{+13.01}_{-11.66}$
NGVS footprint[a] red sequence	$-1.36^{+0.15}_{-0.12}$	$-16.31^{+0.77}_{-1.07}$	$21.57^{+20.91}_{-12.58}$
NGVS footprint[a] late-type	$-0.98^{+0.06}_{-0.06}$	$-17.36^{+0.26}_{-0.28}$	$64.92^{+13.60}_{-12.50}$

Notes. a = 1 virial radius from M87 and M49.

Table 3. NUV luminosity function in the different cluster substructures.

NUV	Cluster A	Cluster B	W cloud	C + W'	M + LVC	Periphery
−20	–	–	–	–	–	–
−19	–	1	–	–	–	1
−18	2	–	–	–	–	4
−17	13	5	1	3	2	12
−16	9	10	–	4	4	21
−15	25	6	7	7	6	36
−14	26	10	12	4	9	46
−13	34	13	19	8	14	62
−12	38	11	14	6	6	63

Notes. Number of objects.

according to their location in the M_{star} vs. $NUV - i$ diagram using the same selection criteria given in Boselli et al. (2014a). We prefer to select galaxies according to a quantitative colour-stellar mass relation rather than to a subjective morphology classification mainly because of the physical interpretation of this diagram in the framework of galaxy transformation in high-density environments (see Boselli et al. 2014a for details).

Figure 7 shows the NUV luminosity function of the whole cluster separately for galaxies belonging to the red sequence, the green valley, and the blue cloud. The values are given in Table 1, while the parameters of the best fitted Schechter functions are given in Table 2 and are compared in Fig. 8. Figures 7 and 8, and Tables 1 and 2, consistently indicate that at the bright end the NUV luminosity function of the Virgo cluster is dominated by late-type galaxies (the difference in M^* between blue and red galaxies is of ~1 mag), while the increasing number of galaxies at the faint end is mainly due to the red quiescent galaxy population, as already found in other clusters (Cortese et al. 2005,

Table 4. NUV luminosity function: cluster A vs. periphery.

NUV	Cluster A red	Cluster A green	Cluster A blue	Periphery red	Periphery green	Periphery blue
−20	–	–	–	–	–	–
−19	–	–	–	–	–	1
−18	–	–	2	–	–	4
−17	3	2	8	2	–	10
−16	2	1	6	–	5	16
−15	12	6	7	6	1	29
−14	12	6	8	6	8	32
−13	22	7	5	9	12	41
−12	26	8	4	17	14	32

Notes. Number of objects.
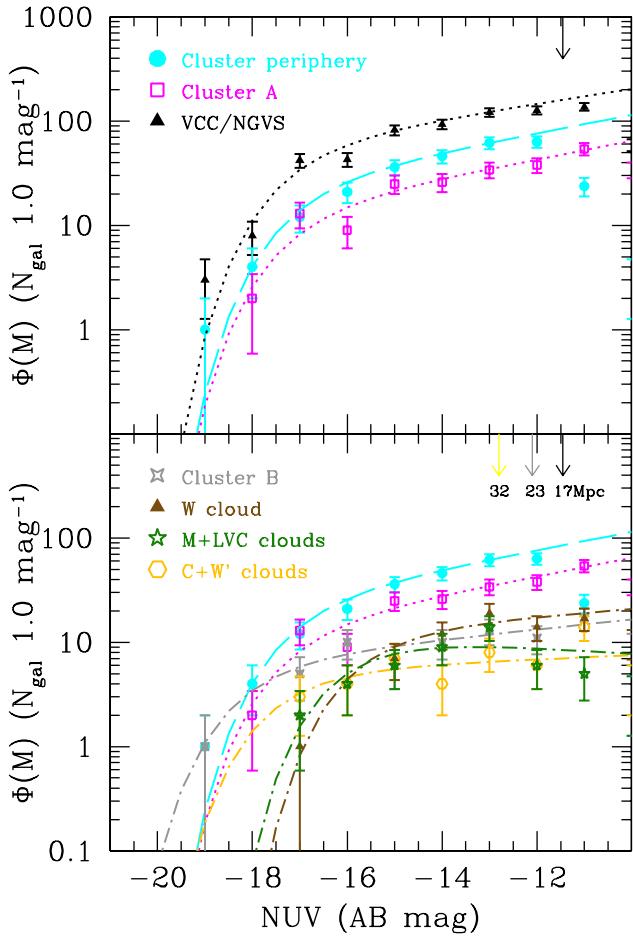
Fig. 5. *Upper panel*: NUV luminosity function of Virgo cluster A (magenta empty squares) and of the cluster periphery (cyan filled dots) are compared to that determined over the $104°^2$ sampled by the VCC and the NGVS survey (black filled triangles). The best fit Schechter functions are shown by the magenta dotted, cyan long dashed, and black dotted lines, respectively. The vertical arrow shows the limit of completeness of the luminosity function. *Lower panel*: the same cluster A and periphery luminosity functions are compared to those determined for cluster B (grey empty stars), W cloud (brown filled triangles), M plus low-velocity clouds (LVC; dark green empty stars), and cluster C plus W' cloud (orange empty hexagons). The vertical arrows show the different limits of completeness for the different cluster substructures: 17 Mpc for cluster A, cluster C, LVC, and the cluster periphery, 23 Mpc for cluster B and W' cloud, 32 Mpc for W and M clouds.

2008). The slope of the early-type red galaxies ($\alpha = -1.37$) is significantly steeper than that of the star forming systems within the blue cloud ($\alpha = -0.94$).
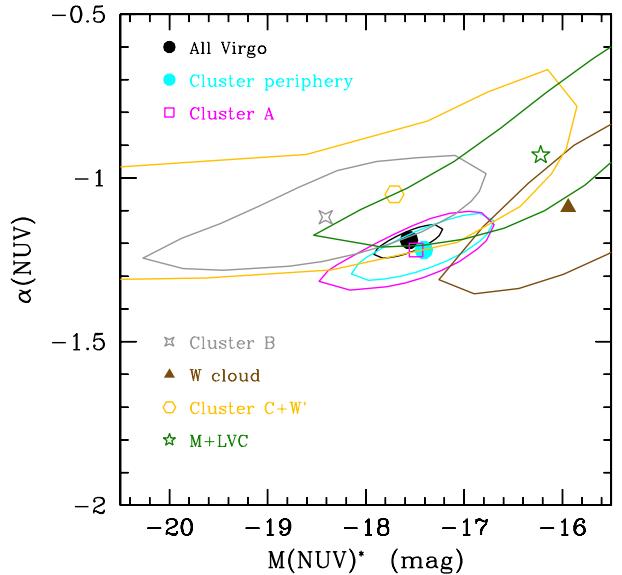
Fig. 6. Comparison of the Schechter function parameters determined for the whole Virgo cluster region (black filled circle), for the cluster periphery (cyan filled circle), cluster A (magenta empty square), cluster B (grey empty star), W cloud (brown filled triangle), cluster C and W' cloud (orange empty hexagon), and M and LVC clouds (dark green empty star). The contours show the 1 sigma probability distribution.

The comparison between the different morphological classes can also be done separately for galaxies located within cluster A and at the periphery of the cluster (Fig. 9; Table 1). The limited number of galaxies prevents an accurate determination of the parameters of the Schechter function for early-type galaxies in the periphery of the cluster.

Despite a significant decrease in the total number of objects, the shape of the NUV luminosity function of red galaxies does not change significantly between cluster A and the periphery. A Kolmogorov-Smirnov test indicates that the probability that the cluster A and the cluster periphery early-type galaxy distributions are driven by the same parent distribution is 11%. Important variations are instead observed in the NUV luminosity function of blue galaxies. There is an evident change in the slope at faint luminosities from $\alpha = -1.10$ in the outskirts of the cluster to $\alpha = -0.76$ in the core of cluster A. In the cluster periphery the NUV luminosity function is dominated by blue galaxies at all luminosities (we note that the value of $\alpha = -1.10$ determined for this category of objects is very close to the value derived in the field by Wyder et al. 2005), while in the core of the cluster it is dominated by the steep rise of red early-type dwarf galaxies below $NUV > -14$ mag ($\alpha = -1.25$). This result does
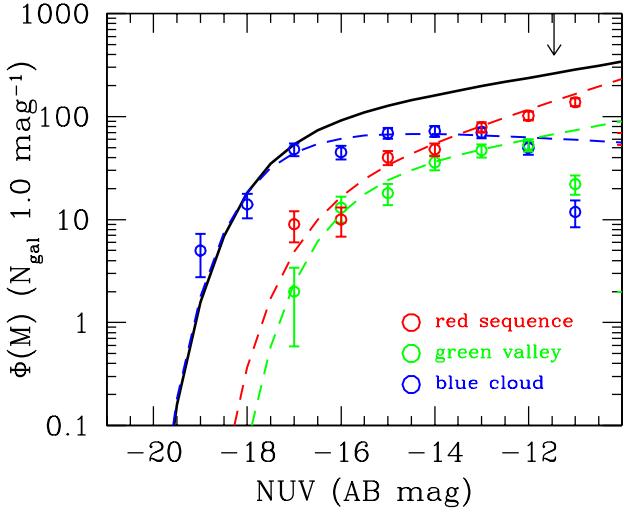
Fig. 7. NUV luminosity function of the Virgo cluster for galaxies of different morphological type selected according to their *NUV − i* colour, as described in Boselli et al. (2014a). Red, green, and blue symbols stand for galaxies in the red sequence, green valley, and blue could, respectively. The black solid line shows the total NUV luminosity function of the cluster. The vertical arrow shows the completeness limit of the survey.

Fig. 8. Comparison of the Schechter function parameters determined for the whole Virgo cluster region (black symbol) and for galaxies belonging to the red sequence, green valley, and blue cloud, as defined in Boselli et al. (2014a). The contours show the 1 sigma probability distribution.

not necessary contradict what was found in the Coma cluster, i.e. that the shape of the NUV luminosity function of early- and late-type galaxies does not change in the clustercentric distance range $0.5° < R < 2°$ (Cortese et al. 2008). Indeed, once considered in terms of virial radii, this range ($0.3 < R/R_{\rm Vir} < 1.2$) does not match the one considered in this analysis (cluster A: $R/R_{\rm Vir} < 0.5$; cluster periphery: $R/R_{\rm Vir} > 1.1$).

4.4. Star formation rate

The UV emission of star forming systems is due to young and massive stars whose life on the main sequence is relatively short. If the star formation activity of galaxies is fairly constant over timescales as long as the typical age of the (emitting stars (stationarity conditions), UV luminosities corrected for dust attenuation can be converted into SFR (e.g. Kennicutt 1998; Boselli et al. 2009; Boquien et al. 2014). The constant of transformation can be determined using different population synthesis models, and depends on the assumed IMF and metallicity (e.g. Boselli 2011). The NUV emission of late-type galaxies is principally due to stars with a typical age of ~150 Myr (Boissier 2013). These timescales are comparable to the timescales for the observed variations in the star formation activity of cluster galaxies. In these objects the interaction with the hostile cluster environment is able to remove a large fraction of the atomic and molecular gas content (Fumagalli et al. 2009; Boselli et al. 2014b) on relatively short timescales (~100–700 Myr, Boselli et al. 2006, 2008a; Tonnesen & Bryan 2009), thus quenching the activity of star formation. This process is particularly efficient in dwarf systems where the shallow potential well of the galaxies cannot keep the gas reservoir anchored to the disc even in the central regions. The stationarity conditions required for transforming NUV luminosities into SFR are thus not necessarily satisfied. For comparison with other works and keeping in mind this caveat, however, we can try to convert the NUV luminosities corrected for dust attenuation (see Sect. 2) into SFR. For the reason mentioned above (quenching of the star formation activity of cluster galaxies), by using NUV data we expect
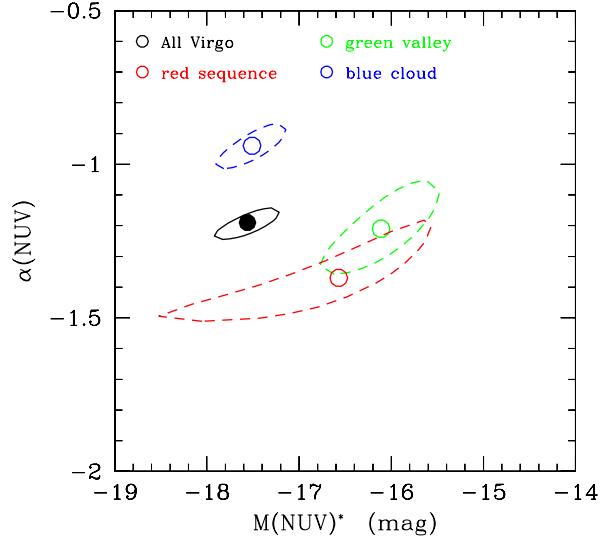
to overestimate the present day star formation activity of cluster galaxies, in particular in low luminosity objects.

Figure 10 shows the distribution of the SFR determined for late-type galaxies in the Virgo cluster region (Table 5). This distribution has been determined for galaxies in the blue sequence only (upper panel), or for all star forming galaxies (blue sequence and green valley; lower panel) separately for objects situated within cluster A and at the periphery of the cluster. We do not consider here red quiescent galaxies where the UV emission can be due to evolved stars (e.g. O'Connell 1999; Boselli et al. 2005b). The SFR luminosity distribution of both the blue sequence and of all the star forming galaxies at the periphery of the Virgo cluster is similar to that determined for the field using SDSS and GAMA data (Gunawardhana et al. 2013). It is, however, significantly steeper than the that determined for galaxies located within cluster A, consistent with what is shown in Fig. 9. These distributions are fitted with a Schechter function whose parameters are given in Table 6.

5. Discussion

There might be several origins of the differences observed with other clusters and with the field (Sect. 4.1), as already discussed in Boselli et al. (2011):

a) A different sampling in absolute magnitude for the different clusters and the field. The limiting magnitude in Coma, A1367, and Shapley is only $NUV \leq -14.5$ vs. $\simeq -11.5$ in Virgo. If we limit the comparison with these clusters down to the limiting magnitude of $NUV \leq -14.5$ mag, however, we do not observe any significant change in the slope α of the Schechter function in Virgo. Given the degeneracy between the Schechter parameters α and M^* it is difficult to establish whether the position of the knee of the Schechter function is significantly different in the various clusters and in the field or is just due to their steeper slope at the faint end. We note, however, that clusters such as Coma and A1367 contain a number of gas-rich late-type systems characterised by a strong activity of star formation probably induced by

Table 5. SFR luminosity function.

log *SFR*	Cluster A blue+green	Periphery blue+green	Cluster A blue	Periphery blue
−2.5	12	68	4	51
−2.0	17	52	10	41
−1.5	15	44	7	39
−1.0	6	24	1	21
−0.5	10	17	9	13
0	7	11	6	9
0.5	4	4	4	4
1.0	0	1	0	1

Notes. Number of objects.
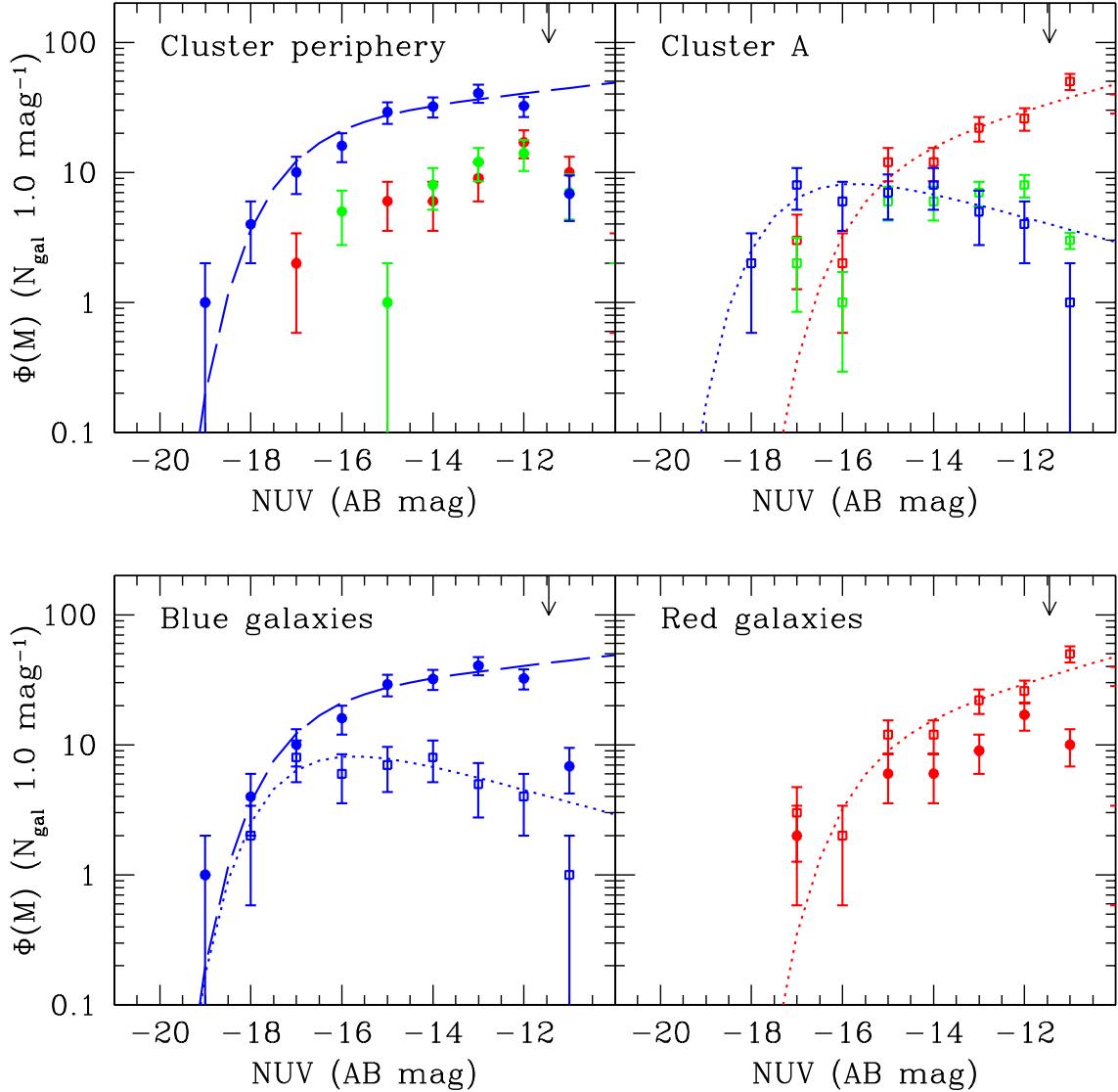
Fig. 9. *Upper panels*: NUV luminosity function of galaxies in the Virgo cluster periphery (*left*, filled dots) and in the core of cluster A (*right*, empty squares). Red symbols are for galaxies belonging to the red sequence, green symbols for galaxies in the green valley, and blue symbols for galaxies in the blue cloud. *Lower panels*: NUV luminosity function of cluster A (empty squares) and cluster periphery (filled dots) galaxies in the blue (*left*) and red (*right*) sequences. The red and blue lines give the best fit Schechter functions derived for the different samples. The different luminosity functions have been normalised to approximately the same number of objects.

their interaction with the surrounding intracluster medium (Iglesias-Paramo et al. 2004). These galaxies were first discovered by Bothun & Dressler (1986) in the Coma cluster and are typical of unrelaxed clusters such as A1367. Typical examples are the CGCG 97-73, 97-79, and 97-87 galaxies at the north-west periphery of the cluster (Gavazzi et al. 2001). Similar objects are apparently lacking in Virgo as revealed by the complete Hα narrow band imaging survey of
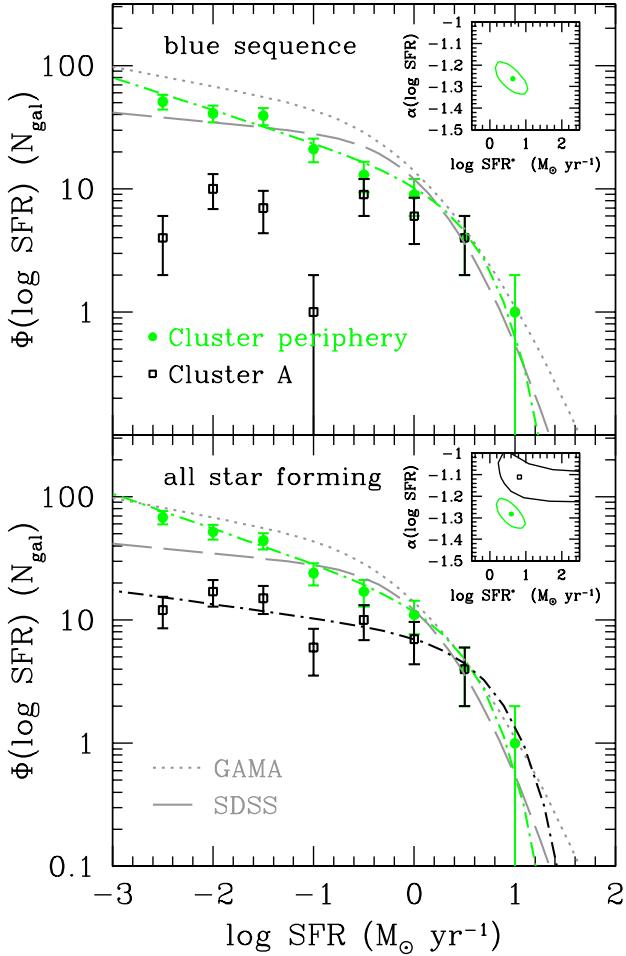
Fig. 10. SFR luminosity function of galaxies in the cluster periphery (green filled dots) and in cluster A (black empty squares) derived from the NUV luminosity function of galaxies in the blue sequence (*upper panel*) and of all star forming objects, including those in the green valley (*lower panel*). These SFR luminosity functions (green dot-dashed lines for the periphery and black for cluster A) are compared to those derived by Gunawardhana et al. (2013) for the GAMA (grey dotted line) and the SDSS (grey long dashed line) samples. The different luminosity functions have been normalised to approximately the same number of objects for comparison. The small panels in the *top right* indicate the 1 sigma probability distribution of the fitted Schecheter function parameters.

the cluster (Koopmann et al. 2001; Boselli & Gavazzi 2002; Boselli et al. 2002; Gavazzi et al. 2006).

b) Boselli et al. (2011) invoked a possible bias in the determination of the UV luminosity function in the central 12 deg^2 of Virgo because of the lack of bright galaxies in their sample. The region analysed in this work is ~25 times larger and the number of objects is larger by a factor of ~8 than in that work, making our determination of the NUV luminosity function robust.

c) Possible radial effects in the galaxy distribution. The Coma cluster NUV luminosity function of Cortese et al. (2008) has been determined over an area of 25 Mpc^2, although avoiding the core of the cluster because of the presence of bright stars saturating the detector. On the contrary, the NUV luminosity function of A1367 is limited to the central ~2 Mpc^2, corresponding to ~0.37 R_V. The properties of the fitted Schechter functions of these two clusters, however, are very similar, as depicted in Figs. 3 and 4. If limited to the infalling region

Table 6. Best fitting parameters for the SFR luminosity function.

Sample	α	log SFR^*	ϕ_*
Cluster periphery, blue cloud	$-1.26^{+0.05}_{-0.05}$	$0.64^{+0.27}_{-0.31}$	$8.82^{+4.66}_{-3.09}$
Cluster periphery, all star forming	$-1.28^{+0.05}_{-0.04}$	$0.60^{+0.25}_{-0.27}$	$10.26^{+4.96}_{-3.47}$
Cluster A, all star forming	$-1.11^{+0.08}_{-0.08}$	$0.83^{+0.64}_{-0.43}$	$6.58^{+4.09}_{-5.07}$

in the south-west of Coma, where UV data are available for galaxies down to $NUV = -10.5$, Hammer et al. (2012) determined a slope $\alpha = -1.39$, slightly flatter than the one determined by Cortese et al. (2008) in the outer regions but still significantly steeper than the one determined in this work. Furthermore, we have shown that the shape of the fitted Schechter function does not change significantly from the core to the periphery of the cluster, corroborating the idea that radial effects are not important.

d) The determination of the slope of the UV luminosity function at the faint end strongly depends on poorly constrained statistical corrections in clusters other than Virgo (e.g. Rines & Geller 2008; see Fig. 2). At the limiting observed magnitude of 21 mag in the NUV used by Cortese et al. (2008) not all galaxies have an optical counterpart necessary for the star-galaxy identification on the SDSS (Voyer et al. 2014). In the Coma cluster and in the Shapley supercluster the completeness in redshift is present only down to $NUV = -17$, and drops to ≲20% at the limiting absolute mag of $NUV = -14$ (Fig. 2). In Hammer et al. (2012) the UV selected galaxies ($NUV \leq 24.5$ mag) must have a SDSS optical counterpart with $r \leq 21.2$ mag. With this condition all star forming objects are automatically excluded from the sample. Although we cannot exclude real differences in the luminosity distribution of galaxies within these clusters, which are known to be characterised by different intrinsic properties (relaxation state and presence of substructures, spiral fraction, density of the intracluster medium and X-ray properties), it is conceivable that part of the observed differences results from the uncertain statistical corrections required in clusters more distant than Virgo.

The NUV luminosity function determined in this work can also be compared to those obtained at other frequencies in the Virgo cluster. As summarised in Boselli & Gavazzi (2014), these are now available only in optical bands (Sandage et al. 1985, photographic *B*-band; Trentham & Hodgkin 2002, *B*-band; Rines & Geller 2008, *r*-band; Lieder et al. (2012), *V*- and *I*-bands). We can compare our results to those obtained by Rines & Geller (2008) in the *r*-band within 1 Mpc from M87 since their sampled region closely corresponds to the cluster A definition adopted in this work (<0.8 Mpc). Furthermore both works use membership criteria based on spectroscopic redshifts and are thus only marginally affected by statistical corrections. The fit with a Schechter function done by Rines & Geller (2008) gives $M_R^* = -21.32$ and $\alpha = -1.28$. Considering a typical $NUV - r$ colour of ~5.5, 4.5, and 3.5 mag for massive red sequence, green valley, and blue cloud galaxies as derived from the $NUV - i$ colour–magnitude relation of Boselli et al. (2014a) and the typical $r - i$ colours of nearby galaxies (Fukugita et al. 1995), we can tentatively transform the NUV luminosity function of cluster A given in Table 2 in a *r*-band luminosity function. We thus expect that the derived *r*-band luminosity function is dominated by the early-type galaxy population with M_r^* and α values close to those obtained by Rines & Geller (2008). We note, however, that this

is a very crude approximation since i) the colour of galaxies is luminosity-dependent and ii) the *r*- and NUV-bands are sensitive to very different stellar populations, thus selection effects should be important.

The variations of the NUV luminosity function with morphological type and cluster location can be analysed in the framework of galaxy evolution in high-density environments (see Boselli & Gavazzi 2006, 2014, for a review). The fact that the NUV luminosity function does not change significantly in terms of faint end slope going from the cluster core ($\leq 0.5\,R_{\rm vir}$) to the outskirts ($\gtrsim 1.1\,R_{\rm vir}$) and to the field, suggests that whatever perturbing mechanism is acting on low-luminosity galaxies entering the cluster, this does not change their number per unit NUV luminosity. The interpretation of this observational result, however, is not straightforward since the different environmental processes can modify in a complex way both the number of objects and the luminosity of the perturbed galaxies. As a first indication we would be tempted to exclude for Virgo the combined effect of dwarf tidal disruption in the core of the cluster and galaxy harassment invoked by Popesso et al. (2006), Barkhouse et al. (2007), and de Filippis et al. (2011) to explain the observed flattening in the core and the steepening in the periphery in the optical luminosity function of nearby clusters. We do not observe in Virgo any radial variations of the luminosity function either in the NUV or in the *r*-band (Rines & Geller 2008). On the contrary, our results seem consistent with a mild transformation of star forming systems into quiescent dwarf elliptical galaxies after a rapid ram pressure stripping event as first proposed by Boselli et al. (2008a,b). Because of their shallow potential well, low-luminosity star forming galaxies easily lose their gas because of ram pressure stripping and quench their activity of star formation on timescales of $\lesssim 1$ Gyr. This happens at the periphery of the cluster once they encounter the intergalactic medium trapped within the potential of the cluster. Because this timescale is relatively short compared to the crossing time of the cluster (~ 1.7 Gyr), these newly accreted galaxies are already red when they reach the cluster core (Boselli et al. 2014a). This effect is consistent with the observed reversed shape of the NUV luminosity function of red and blue galaxies in the cluster core and at the periphery (Fig. 9). It is also consistent with the spectrophotometric, structural (Boselli et al. 2008a,b), and kinematic (Toloba et al. 2009, 2011, 2012, 2015) properties of Virgo cluster dwarf elliptical galaxies that were extensively reviewed in Boselli & Gavazzi (2014).

The perturbations induced by the cluster environment on the star formation activity of galaxies are obviously more efficient in low-mass systems than in massive spirals. In massive objects the steep potential well can retain some gas in the inner regions producing radially truncated discs as in the case of NGC 4569 (Boselli et al. 2006). The timescale necessary for the total ablation of the atomic and molecular gas here is longer than in dwarfs as indicated both by observations and hydrodynamic simulations (Roediger & Bruggen 2007; Tonnesen & Bryan 2009; Hughes & Cortese 2009; Cortese & Hughes 2009; Fumagalli et al. 2009; Gavazzi et al. 2013a,b; Boselli et al. 2014a,b). The observed increasing difference with decreasing SFR in the SFR luminosity function of the Virgo cluster shown in Fig. 10 is further statistical evidence of this phenomenon.

6. Conclusion

We have determined the properties of the NUV luminosity function of the Virgo cluster over ~ 300 deg^2 ($\sim$up to 1.8 virial radii) thanks to the GUViCS survey using a complete sample of ~ 833 galaxies, out of which 808 identified as Virgo members using spectroscopic data and 10 with optical scaling relations, down to the 100% completeness limit of $NUV = -11.5$. The results of this analysis can be summarised as follows:

1) The NUV luminosity function can be represented by a Schechter function with $M^* = -17.56$ and $\alpha = -1.19$. M^* is $\sim$1–2 mag fainter and the slope significantly flatter than the value found in other clusters. The parameter M^* is only $\sim$0.8 mag fainter and α is comparable to those values determined in the field. The difference with other clusters is probably due to the quite uncertain statistical correction necessary to identify members in clusters at distances higher than Virgo.

2) The NUV luminosity function of galaxies of different morphological types as determined according to their position within the $NUV - i$ vs. The $M_{\rm star}$ relation is significantly different. Late-type galaxies belonging to the blue sequence dominate the bright end of the luminosity function, while their faint end is very flat $\alpha = -0.94$). On the contrary, early-type galaxies belonging to the red sequence dominate the faint end ($\alpha = -1.37$) of the total NUV luminosity function below $NUV \simeq -13$ mag.

3) The overall properties of the NUV luminosity function determined within 0.5 virial radii of cluster A (the main structure of Virgo) and in the cluster periphery (outside ~ 1.1 virial radii) are comparable. In the outskirts of the cluster the NUV luminosity function is comparable to that determined in the field by Wyder et al. (2005). Here it is dominated down to $NUV \simeq -11.5$ by blue galaxies, with a mild rise at faint luminosities ($\alpha = -1.10$). In the cluster core, red quiescent galaxies dominate for $NUV \gtrsim -15$ mag ($\alpha = -1.25$), while the number of star forming systems drops significantly ($\alpha = -0.76$). These observed properties of the NUV luminosity function are consistent with a rapid transformation of star forming galaxies recently entered in the cluster environment after a ram pressure stripping event.

References

Barkhouse, W. A., Yee, H. K. C., & López-Cruz, O. 2007, ApJ, 671, 1471
Binggeli, B., Sandage, A., & Tammann, G. A. 1985, AJ, 90, 1681
Binggeli, B., Sandage, A., & Tammann, G. A. 1988, ARA&A, 26, 509
Boissier, S. 2013, in Planets, Stars and Stellar Systems, Vol. 6: Extragalactic Astronomy and Cosmology, 141
Boissier, S., Boselli, A., Duc, P.-A., et al. 2012, A&A, 545, A142
Boissier, S., Boselli, A., Voyer, E., et al. 2015, A&A, 579, A29
Boquien, M., Buat, V., & Perret, V. 2014, A&A, 571, A72
Boselli, A. 2011, A Panchromatic View of Galaxies, Practical Approach Book (Berlin: Wiley-VCH)
Boselli, A., & Gavazzi, G. 2002, A&A, 386, 124
Boselli, A., & Gavazzi, G. 2006, PASP, 118, 517
Boselli, A., & Gavazzi, G. 2014, A&ARv, 22, 74
Boselli, A., Iglesias-Páramo, J., Vílchez, J. M., & Gavazzi, G. 2002, A&A, 386, 134
Boselli, A., Cortese, L., Deharveng, J. M., et al. 2005a, ApJ, 629, L29
Boselli, A., Boissier, S., Cortese, L., et al. 2005b, ApJ, 623, L13
Boselli, A., Boissier, S., Cortese, L., et al. 2006, ApJ, 651, 811
Boselli, A., Boissier, S., Cortese, L., & Gavazzi, G. 2008a, ApJ, 674, 742
Boselli, A., Boissier, S., Cortese, L., & Gavazzi, G. 2008b, A&A, 489, 1015
Boselli, A., Boissier, S., Cortese, L., et al. 2009, ApJ, 706, 1527
Boselli, A., Boissier, S., Heinis, S., et al. 2011, A&A, 528, A107
Boselli, A., Voyer, E., Boissier, S., et al. 2014a, A&A, 570, A69
Boselli, A., Cortese, L., Boquien, M., et al. 2014b, A&A, 564, A67
Bothun, G. D., & Dressler, A. 1986, ApJ, 301, 57
Byrd, G., & Valtonen, M. 1990, ApJ, 350, 89
Cortese, L., & Hughes, T. M. 2009, MNRAS, 400, 1225
Cortese, L., Boselli, A., Gavazzi, G., et al. 2005, ApJ, 623, L17
Cortese, L., Gavazzi, G., & Boselli, A. 2008, MNRAS, 390, 1282
Cowie, L. L., & Songaila, A. 1977, Nature, 266, 501
D'Abrusco, R., Staiano, A., Longo, G., et al. 2007, ApJ, 663, 752
Davies, J. I., Baes, M., Bendo, G. J., et al. 2010, A&A, 518, L48
de Filippis, E., Paolillo, M., Longo, G., et al. 2011, MNRAS, 414, 2771
Dressler, A. 1980, ApJ, 236, 351
Dressler, A. 2004, in Clusters of Galaxies: Probes of Cosmological Structure and Galaxy Evolution (CUP), 206
Dressler, A., Oemler, A., Jr., Couch, W. J., et al. 1997, ApJ, 490, 577
Drinkwater, M. J., Jones, J. B., Gregg, M. D., & Phillipps, S. 2000, PASA, 17, 227
Ferrarese, L., Côté, P., Cuillandre, J.-C., et al. 2012, ApJS, 200, 4
Ferrarese, L., Côté, P., MacArthur, L., et al. 2015, ApJS, submitted
Fitzpatrick, E. L., & Massa, D. 2007, ApJ, 663, 320
Fukugita, M., Shimasaku, K., & Ichikawa, T. 1995, PASP, 107, 945
Fumagalli, M., Krumholz, M. R., Prochaska, J. X., Gavazzi, G., & Boselli, A. 2009, ApJ, 697, 1811
Gavazzi, G., Boselli, A., Scodeggio, M., Pierini, D., & Belsole, E. 1999, MNRAS, 304, 595
Gavazzi, G., Boselli, A., Mayer, L., et al. 2001, ApJ, 563, L23
Gavazzi, G., Boselli, A., Donati, A., Franzetti, P., & Scodeggio, M. 2003, A&A, 400, 451
Gavazzi, G., Boselli, A., Cortese, L., et al. 2006, A&A, 446, 839
Gavazzi, G., Fumagalli, M., Fossati, M., et al. 2013a, A&A, 553, A89
Gavazzi, G., Savorgnan, G., Fossati, M., et al. 2013b, A&A, 553, A90
Giovanelli, R., Haynes, M. P., Kent, B. R., et al. 2005, AJ, 130, 2598
Gunawardhana, M. L. P., Hopkins, A. M., Bland-Hawthorn, J., et al. 2013, MNRAS, 433, 2764
Gunn, J. E., & Gott, J. R., III 1972, ApJ, 176, 1
Haines, C. P., Busarello, G., Merluzzi, P., et al. 2011, MNRAS, 412, 127
Hammer, D. M., Hornschemeier, A. E., Salim, S., et al. 2012, ApJ, 745, 177
Hao, C.-N., Kennicutt, R. C., Johnson, B. D., et al. 2011, ApJ, 741, 124
Hilker, M., Infante, L., Vieira, G., Kissler-Patig, M., & Richtler, T. 1999, A&AS, 134, 75
Hughes, T. M., & Cortese, L. 2009, MNRAS, 396, L41
Iglesias-Páramo, J., Boselli, A., Gavazzi, G., & Zaccardo, A. 2004, A&A, 421, 887
Ilbert, O., Tresse, L., Zucca, E., et al. 2005, A&A, 439, 863
James, F., & Roos, M. 1995, MINUIT Function Minimization and Error Analysis, Version 95.03 (CERN Program Library D506)
Kennicutt, R. C., Jr. 1998, ARA&A, 36, 189
Kim, S., Rey, S.-C., Jerjen, H., et al. 2014, ApJS, 215, 22
Koda, J., Yagi, M., Yamanoi, H., & Komiyama, Y. 2015, ApJ, 807, L2
Koopmann, R. A., Kenney, J. D. P., & Young, J. 2001, ApJS, 135, 125
Larson, R. B., Tinsley, B. M., & Caldwell, C. N. 1980, ApJ, 237, 692
Lieder, S., Lisker, T., Hilker, M., Misgeld, I., & Durrell, P. 2012, A&A, 538, A69
McLaughlin, D. E. 1999, ApJ, 512, L9
Mei, S., Blakeslee, J. P., Côté, P., et al. 2007, ApJ, 655, 144
Merritt, D. 1983, ApJ, 264, 24
Mihos, J. C., Durrell, P. R., Ferrarese, L., et al. 2015, ApJ, 809, L21
Moore, B., Lake, G., & Katz, N. 1998, ApJ, 495, 139
Morrissey, P., Conrow, T., Barlow, T. A., et al. 2007, ApJS, 173, 682
Nulsen, P. E. J. 1982, MNRAS, 198, 1007
O'Connell, R. W. 1999, ARA&A, 37, 603
Popesso, P., Biviano, A., Böhringer, H., & Romaniello, M. 2006, A&A, 445, 29
Raichoor, A., Mei, S., Erben, T., et al. 2014, ApJ, 797, 102
Rines, K., & Geller, M. J. 2008, AJ, 135, 1837
Roediger, E., & Brüggen, M. 2007, MNRAS, 380, 1399
Sandage, A., Binggeli, B., & Tammann, G. A. 1985, AJ, 90, 1759
Schlegel, D. J., Finkbeiner, D. P., & Davis, M. 1998, ApJ, 500, 525
Toloba, E., Boselli, A., Gorgas, J., et al. 2009, ApJ, 707, L17
Toloba, E., Boselli, A., Cenarro, A. J., et al. 2011, A&A, 526, A114
Toloba, E., Boselli, A., Peletier, R. F., et al. 2012, A&A, 548, A78
Toloba, E., Guhathakurta, P., Boselli, A., et al. 2015, ApJ, 799, 172
Tonnesen, S., & Bryan, G. L. 2009, ApJ, 694, 789
Trentham, N., & Hodgkin, S. 2002, MNRAS, 333, 423
van Dokkum, P. G., Romanowsky, A. J., Abraham, R., et al. 2015, ApJ, 804, L26
Voyer, E. N., Boselli, A., Boissier, S., et al. 2014, A&A, 569, A124
Whitmore, B. C., Gilmore, D. M., & Jones, C. 1993, ApJ, 407, 489
Wyder, T. K., Treyer, M. A., Milliard, B., et al. 2005, ApJ, 619, L15
Zhang, H.-X., Peng, E. W., Côté, P., et al. 2015, ApJ, 802, 30